Effects of Cloud Parameterization on the Simulation of Climate Changes in the GISS GCM

MAO-SUNG YAO

Science Systems and Applications, Inc., NASA/Goddard Space Flight Center, Institute for Space Studies, New York, New York

ANTHONY D. DEL GENIO

NASA/Goddard Space Flight Center, Institute for Space Studies, New York, New York

(Manuscript received 13 January 1998, in final form 23 April 1998)

ABSTRACT

Climate changes obtained from five doubled CO_2 experiments with different parameterizations of large-scale clouds and moist convection are studied by use of the Goddard Institute for Space Studies (GISS) GCM at 4° lat × 5° long resolution. The baseline for the experiments is GISS Model II, which uses a diagnostic cloud scheme with fixed optical properties and a convection scheme with fixed cumulus mass fluxes and no downdrafts. The global and annual mean surface air temperature change (ΔT_s) of 4.2°C obtained by Hansen et al. using the Model II physics at 8° lat × 10° long resolution is reduced to 3.55°C at the finer resolution. This is due to a significant reduction of tropical cirrus clouds in the warmer climate when a finer resolution is used, despite the fact that the relative humidity increases there with a doubling of CO_2. When the new moist convection parameterization of Del Genio and Yao and prognostic large-scale cloud parameterization of Del Genio et al. are used, ΔT_s is reduced to 3.09°C from 3.55°C. This is the net result of the inclusion of the feedback of cloud optical thickness and phase change of cloud water, and the presence of areally extensive cumulus anvil clouds. Without the optical thickness feedback, ΔT_s is further reduced to 2.74°C, suggesting that this feedback is positive overall. Without anvil clouds, ΔT_s is increased from 3.09° to 3.7°C, suggesting that anvil clouds of large optical thickness reduce the climate sensitivity. The net effect of using the new large-scale cloud parameterization without including the detrainment of convective cloud water is a slight increase of ΔT_s from 3.56° to 3.7°C. The net effect of using the new moist convection parameterization without anvil clouds is insignificant (from 3.55° to 3.56°C). However, this is a result of a combination of many competing differences in other climate parameters. Despite the global cloud cover decrease simulated in most of the experiments, middle- and high-latitude continental cloudiness generally increases with warming, consistent with the sense of observed twentieth-century cloudiness trends; an indirect aerosol effect may therefore not be the sole explanation of these observations.

An analysis of climate sensitivity and changes in cloud radiative forcing (CRF) indicates that the cloud feedback is positive overall in all experiments except the one using the new moist convection and large-scale cloud parameterization with prescribed cloud optical thickness, for which the cloud feedback is nearly neutral. Differences in ΔCRF among the different experiments cannot reliably be anticipated by the analogous differences in current climate CRF. The meridional distribution of ΔCRF suggests that the cloud feedback is positive mostly in the low and midlatitudes, but in the high latitudes, the cloud feedback is mostly negative and the amplification of ΔT_s is due to other processes, such as snow/ice–albedo feedback and changes in the lapse rate. The authors' results suggest that when a sufficiently large variety of cloud feedback mechanisms are allowed for, significant cancellations between positive and negative feedbacks result, causing overall climate sensitivity to be less sensitive to uncertainties in poorly understood cloud physics. In particular, the positive low cloud optical thickness correlations with temperature observed in satellite data argue for a minimum climate sensitivity higher than the 1.5°C that is usually assumed.

1. Introduction

The effect of cloud feedbacks is one of the major uncertainties in the study of climate change. Clouds regulate the radiative heating through their albedo effect, which tends to cool the atmosphere–surface, and through their greenhouse effect, which traps the longwave radiation and tends to warm the atmosphere–surface. Because of the poorly understood, multiscale nature of cloud formation and microphysical processes, different assumptions about the parameterization of convective and large-scale clouds in climate models appear to produce a threefold variation in one measure of global climate sensitivity (Cess et al. 1990).

Notable cloud feedbacks involve changes in cloud

Corresponding author address: Dr. Anthony D. Del Genio, NASA/GISS, 2880 Broadway, New York, NY 10025.
E-mail: delgenio@giss.nasa.gov

height, cloud cover, and cloud optical thickness. Cloud height appears to have a positive feedback for models with prescribed optical thickness decreasing with height. High clouds tend to increase while low and middle clouds tend to decrease by a larger amount in the majority of doubled CO_2 experiments, producing a positive cloud cover feedback too (e.g., Hansen et al. 1984; Wetherald and Manabe 1986). Recent cloud parameterizations (e.g., Sundqvist 1978; Smith 1990; Roeckner et al. 1987; Del Genio et al. 1996; Fowler et al. 1996) include a prognostic cloud water variable so that the cloud optical thickness (or cloud albedo and emissivity) can be predicted. However, depending on the model's treatments, the optical thickness feedback can be positive, negative, or nearly neutral.

Comparison of climate sensitivities with different cloud parameterizations can help identify the sign and magnitude of individual cloud feedbacks and suggest areas of needed improvement in the parameterization. Cess et al. (1990, 1996) performed climate sensitivity experiments using many different general circulation models (GCMs) by increasing/decreasing sea surface temperature 2°C as a surrogate for a forced climate change. While this approach produces results quickly, it may not generate a true sensitivity applicable to actual climate change scenarios, since horizontal variations of sea surface temperature apparently have a profound effect on the climate sensitivity (Senior and Mitchell 1993; Del Genio et al. 1996). Mitchell et al. (1989) and Senior and Mitchell (1993) conducted four doubled CO_2 experiments using different cloud parameterizations with a single GCM. They found that the presence or absence of cloud microphysical and optical thickness feedbacks can cause the global warming of the surface air temperature to range from 1.9°C to 5.4°C. Li and Le Treut (1992), using the SST perturbation approach, showed that changing the temperature of the ice–liquid threshold can change the sign of the cloud optical thickness feedback. Using a single GCM has the advantage of avoiding the effect on the climate sensitivity of differences in other physics and dynamics treatments that exists in Cess et al.'s study; on the other hand, the results from any single model are not applicable to every other model and should be assessed only in light of comparisons with observations.

In this paper, we perform a series of doubled CO_2 experiments with the Goddard Institute for Space Studies (GISS) GCM to identify the effects on the climate sensitivity of different elements of its new parameterizations of large-scale clouds and moist convection. Specifically, we focus on the effects of cloud water–optical thickness feedbacks in stratiform clouds and in anvil clouds that are generated by the moist convection scheme. We describe the model and experiments in section 2. In section 3, we show the results of simulations of the current climate. In section 4, we compare the climate changes resulting from doubling CO_2. We analyze the climate sensitivity and changes of cloud radiative forcing (CRF) in section 5. Section 6 is a discussion of the implications of our results, to the extent that conclusions can be drawn from a single model.

2. The model and experiments

a. Relevant features of the GCM

Except for the parameterizations of large-scale clouds and moist convection we use the GISS Model II of Hansen et al. (1983). For the large-scale cloud parameterization, we use the prognostic scheme of Del Genio et al. (1996); for moist convection, we use the parameterization described in Del Genio and Yao (1993). We describe below those parts of the parameterizations that are most directly related to the experiments conducted here.

To parameterize large-scale cloud formation, Del Genio et al. (1996) follow the approach of Sundqvist et al. (1989). A grid box is divided into a cloudy part, of cloud fraction b, with relative humidity $(\mathrm{RH_S}) = 1$, and a clear part $(1 - b)$, where

$$b = (\mathrm{RH} - \mathrm{RH}_o)/(\mathrm{RH_S} - \mathrm{RH}_o), \tag{1}$$

where RH is the grid-box relative humidity, and $\mathrm{RH}_o = \mathrm{RH}_{oo} + b(\mathrm{RH}_S - \mathrm{RH}_{oo})$ is the clear region relative humidity. Here, $\mathrm{RH}_{oo} = 0.6$ is the threshold relative humidity for large-scale clouds to form. A continuity equation for the cloud water content (m) is used, which includes the effect of condensation of water vapor, evaporation of cloud water and rainwater, the conversion of cloud water to precipitation, and the subgrid-scale dynamical source/sink of cloud water due to convective condensate detrainment and cloud-top entrainment instability.

Both liquid and ice phases are allowed to occur in the model, but only one phase exists in a grid box at a given time. The phase of a grid box is initially determined by a smoothly varying probability function of the temperature T, but subsequent glaciation of supercooled water when ice precipitates from above is also possible (Del Genio et al. 1996).

The cloud visible optical thickness is calculated by

$$\tau = 3\mu\Delta Z/2\rho_w r_e, \tag{2}$$

where $\mu = m\rho/b$ is the cloud water density, ρ is the air density, ρ_w is the water density, ΔZ is the cloud physical thickness, and $r_e \simeq 1.3 \times r$, the effective radius of the droplet size distribution (Hansen and Travis 1974) is proportional to the volume-weighted mean droplet radius r. The value of ΔZ can be less than the GCM-layer thickness according to the moist stability of the layer. Once the visible τ is estimated, infrared emissivity is then determined according to the spectral dependence predicted by Mie theory (Hansen et al. 1983), guaranteeing self-consistent shortwave and longwave radiative properties. For evaluating r_e, we assume a constant cloud droplet concentration N, a reference droplet radius

r_o, and a reference cloud water content μ_o. For water cloud, we use $r_o = 10$ μm at $\mu_o = 0.25$ gm^{-3} (corresponding to $N \simeq 60$ cm^{-3}) over ocean. Over land, where there are more cloud condensation nuclei (CCN), we set $r_o = 7$ μm ($N \simeq 170$ cm^{-3}) instead. For ice clouds, we use $r_o = 25$ μm at $\mu_0 = 4.2 \times 10^{-3}$ gm^{-3} ($N \simeq 0.06$ cm^{-3}). Due to the onset of precipitation, when $\mu > \mu_r$, $r = r(\mu_r)$, where μ_r is a critical cloud water content for the onset of rapid conversion of cloud water to precipitation. We use $\mu_r = 0.5$ gm^{-3} for liquid clouds over ocean, 1.0 gm^{-3} for liquid clouds over land, and 0.1 gm^{-3} for ice clouds (the same values as are used to determine when autoconversion becomes important). From (2), we see that the dependence of τ is complex and not a linear function of temperature; in fact, $d\tau/dT$ can and does change sign in the model, a point to which we will return later.

By comparison, Model II uses a much simpler diagnostic large-scale cloud parameterization. Cloud cover depends on the saturated fraction of the grid box, determined by assuming a subgrid-scale temperature distribution whose width is related to the magnitude of resolved temperature variances at the same latitude. Cloud optical thicknesses are prescribed as an increasing function of pressure; all clouds colder than -15°C are assumed to be optically thin ($\tau = 1/3$) cirrus. Condensation is evaluated relative to water saturation at temperatures > -40°C, and relative to ice saturation at colder temperatures; implications of this choice for climate sensitivity are discussed in section 4. This parameterization uses a 5-h time step (the same as is used in the radiation subroutine) as opposed to 1 h in the new parameterization and tends to generate higher humidity and cloud cover in places where convective drying is weak/absent.

The parameterization of moist convection of Del Genio and Yao (1993) assesses instability based on the moist static energy of a parcel lifted one model layer and calculates the convective updraft mass and compensating environmental subsidence by requiring that neutral stability be restored at cloud base after the convection occurs (Yao and Del Genio 1989); this produces behavior consistent with the quasi-equilibrium assumption of Arakawa and Schubert (1974). Multiple cloud bases are permitted. Once convection takes place, two convective plumes are allowed to exist simultaneously per cloud base level, one nonentraining and the other entraining. Downdrafts may exist with the convective updrafts (Del Genio and Yao 1988), partly replacing environmental subsidence. The parameterization allows a fraction of the condensate obtained from the deep convection to detrain into the environment and form anvil clouds. The detrained condensate then combines with any anvil cloud water generated by large-scale cloud formation in the same grid box. The optical thickness of anvil clouds is predicted by (2), and the cloud cover of anvil clouds in the absence of large-scale cloud is $10C_m$, where C_m is the ratio of the convective mass to the grid-box air mass. The optical thickness for the nonanvil portion of convection is prescribed as in Hansen et al. (1983), and the cloud cover is C_m.

The Model II cumulus parameterization is a similar mass flux scheme but is simpler than the new scheme in the following ways: 1) $C_m = 0.5$, independent of the magnitude of instability; 2) only one plume (nonentraining) exists for a given cloud-base level; 3) downdrafts are not represented; 4) there is no cumulus condensate detrainment and no anvil cloud. $C_m = 0.5$ is excessive and tends to produce a drier lower tropical atmosphere.

The only other difference in model physics relative to Model II is that the effect of sea-ice puddling is crudely estimated (Hansen et al. 1997). When the ground temperature over sea ice is greater than -0.1°C, the sea-ice albedo is set to 0.25 in the visible and 0.1 in the near-infrared. (Model II uses 0.55 and 0.3, respectively).

b. The experiments

A total of five equilibrium doubled CO_2 experiments were conducted (Table 1), all run at 4° lat × 5° long resolution and nine vertical layers. Each experiment ran for 40 yr for both 1× (315 ppm) and 2× (630 ppm) CO_2 concentration. The means of the last 10 yr are generally used in this report. However, the cloud radiative forcing and diagnostics of optical thickness are means of extended 5-yr runs. In conducting the experiments, a mixed layer ocean model was coupled to the atmospheric general circulation model (AGCM), using Q fluxes obtained from the local surface energy imbalance in preliminary 5-yr runs with the sea surface temperature prescribed as in Hansen et al. (1984). Separate Q-flux distributions are calculated for each experiment. The current version of the GCM we use (MODELII′, described below) is very close to planetary and surface energy balance globally, but several of the sensitivity experiments have significant global imbalances (see Table 2). To correct this, incoming solar radiation is modified at the ocean surface as in Hansen et al. (1984). The calculated Q fluxes are local deviations from the global mean energy balance. The experiments are described as follows.

1) MODELII′: similar to GISS Model II of Hansen et al. (1983), but using the new parameterization of large-scale clouds and moist convection.
2) NOTAUFB: similar to MODELII′, but the cloud optical thickness is prescribed to be a fixed function of pressure only, as in Eq. (21) of Hansen et al. (1983).
3) NOANVIL: similar to MODELII′, but without the anvil cloud parameterization. The detrained condensate is assumed to immediately precipitate to the surface, with some evaporation as it falls, and cumulus cloud fraction is not increased by a factor of 10 in the upper troposphere.

TABLE 1. Comparison of physics used in the experiments.

	MODELII′	NOTAUFB	NOANVIL	NEWMC	MODELIIF
Moist convection	new	new	new	new	Model II
Large-scale clouds	prognostic	prognostic	prognostic	diagnostic	diagnostic
Optical thickness	predicted	fixed	predicted	fixed	fixed
Anvil clouds	on	on	off	off	off

4) NEWMC: Model II plus the new moist convection scheme, but without the new prognostic cloud water parameterization and without anvil clouds.
5) MODELIIF: the same as Model II, but at 4° lat × 5° long resolution rather than the 8° lat × 10° long resolution used by Hansen et al. (1984).

The details of the physics used in each experiment are summarized in Table 1. Note that comparing MODELII′ and NOTAUFB, we can identify the effect of cloud optical thickness feedback; comparing MODELII′ and NOANVIL, we can visualize the influence of the anvil clouds parameterization; comparing NOANVIL and NEWMC, we can estimate the effect of the new large-scale clouds parameterization itself; NEWMC differs from MODELIIF only in that it uses the new moist convection parameterization.

3. Comparison of the controls

Del Genio et al. (1996) present a comprehensive description and comparison with observations of the GCM's current climate when the new large-scale clouds and moist convection parameterization were included, although the model version used in that paper contains new versions of dynamics and ground hydrology as well. Here we are primarily concerned with the climate sensitivity differences due to different parameterizations of large-scale clouds and moist convection. Therefore, we show here only those current climate results that exhibit significant differences among the experiments, are directly related to cloud–radiation interaction, and may help explain the differences in climate sensitivity. To further limit the presentation, we mainly show global mean values and zonal means.

Table 2 shows the annual mean and global mean values of current climate parameters. Due to climate drift, one cannot totally explain the differences in surface air temperature (T_s) and ground uppermost layer temperature (T_g) among the controls. Comparing the T_s values in Table 2 with those obtained from runs with specified sea surface temperature, we find that the global climate drift (relative to the preliminary run with prescribed sea surface temperature and sea ice) is about 0.2°–0.3°C when the new moist convection and large-scale clouds parameterization is used. The climate drift becomes more severe (as large as 0.6°C in MODELIIF) when the GISS Model II moist convection–large-scale cloud parameterization is used. The sea-ice cover is in all cases

TABLE 2. Selected global mean and annual mean climate parameters. Here, Q is the absorbed solar radiation, and F is the net longwave radiation. Cloud cover and albedo are in %; radiative and turbulent fluxes are in W m^{-2}.

	MODELII′	NOTAUFB	NOANVIL	NEWMC	MODELIIF
T_s (°C)	13.91	13.34	13.85	13.65	14.44
T_g (°C)	14.80	14.45	14.79	14.90	15.39
Total cloud	57.8	58.5	56.0	49.8	48.6
Low cloud	48.1	49.0	48.1	33.4	33.2
Middle cloud	16.4	16.8	11.9	14.0	15.2
High cloud	16.2	16.0	14.1	25.0	23.7
Planetary albedo	30.71	34.15	29.69	26.84	29.96
Ground albedo	11.24	11.72	11.14	10.63	10.48
Q at TOA	236.9	225.2	240.4	250.2	239.5
F at TOA	−236.0	−238.7	−240.3	−238.7	−225.6
Net radiation at TOA	0.9	−13.5	0.1	11.4	13.8
Q at surface	170.4	157.7	173.6	183.2	173.3
F at surface	−45.7	−43.0	−46.9	−53.2	−49.1
Net radiation at surface	127.7	114.7	126.7	129.9	124.2
Net heat at surface	−0.01	−14.38	−0.98	9.57	12.19
TOA CRF (W m^{-2})	−38.64	−54.05	−38.48	−29.98	−27.58
Shortwave CRF	−56.41	−67.90	−52.85	−43.23	−53.81
Longwave CRF	17.77	13.85	14.37	13.26	26.23
Latent heat flux	−100.4	−102.7	−103.5	−90.4	−88.5
Sensible heat flux	−23.2	−25.2	−23.1	−28.8	−22.6
Precipitation (mm day^{-1})	3.47	3.55	3.58	3.13	3.06
Ocean ice (%)	4.8	4.9	4.7	4.9	4.7
Lapse rate (°C km^{-1})	6.0	6.0	6.02	5.85	5.65
Precipitable water (mm)	25.6	24.7	24.5	24.1	26.9

about 4.8%, which is the value when the sea surface temperature is prescribed. Note that due to the surface solar correction we apply, especially in runs where one feature of the cloud parameterization is turned off, the planetary energy imbalances in Table 2 are not actually applied at the ocean surface, thus limiting the extent of any climate drift.

The T_s of NOTAUFB is notably smaller than those of other controls due to higher albedos and cover of low clouds. The T_s of NEWMC is significantly smaller than that of MODELIIF because when the new moist convection parameterization is used, it produces much smaller convective mass flux near the surface and less heating by the subsidence.

We note that when the new large-scale cloud parameterization is used (MODELII′, NOTAUFB, and NOANVIL), total cloud cover, low cloud cover, precipitation, and evaporation are much higher, while high cloud cover is much less, than when the Model II parameterization is used (NEWMC and MODELIIF). There is no single reason that accounts for these differences totally, since the approach to cloud formation is fundamentally different in the new model. The total cloud amount in the new scheme is highly sensitive to the arbitrarily specified threshold relative humidity, in any case. One important factor is that the Model II large-scale cloud parameterization uses a 5-h time step and tends to generate more high clouds as a result.

The CRF is consistent with the model clouds. The strongest shortwave forcing occurs in association with the high-albedo low clouds of NOTAUFB, and in general the cloudier runs produce the larger shortwave CRF. The longwave CRF of MODELIIF is significantly higher than other controls, which is due to the fact that high clouds generated by the Model II moist convection scheme, which does not allow for dilution by entrainment, tend to occur at higher, colder levels.

Figure 1 shows the meridional distribution of T_s of the controls relative to observations. The T_s of NOANVIL is similar to that of MODELII′, and is not shown. MODELII′ is about 6 K warmer than the observed T_s at the South Pole, about 2 K colder elsewhere in both polar regions, too warm at both sea-ice margins, and too cold in the poorly observed southern midlatitudes, but within 1 K at other latitudes, because the implied ocean heat transports are defined to be consistent with observed sea surface temperatures. In the low latitudes, the differences among the controls are similar to the global means, although slightly smaller, while the differences in the high latitudes become as large as a few degrees centigrade. The snow/ice–albedo interaction, lapse rate, and dynamic transports may contribute to these larger differences. In general the sensitivity tests differ from the data more than does MODELII′.

Since the change of CRF when CO_2 is doubled is a measure of climate sensitivity associated with the cloud feedback, we show the meridional distribution of CRF in Fig. 2. (See section 5 for the method of computing

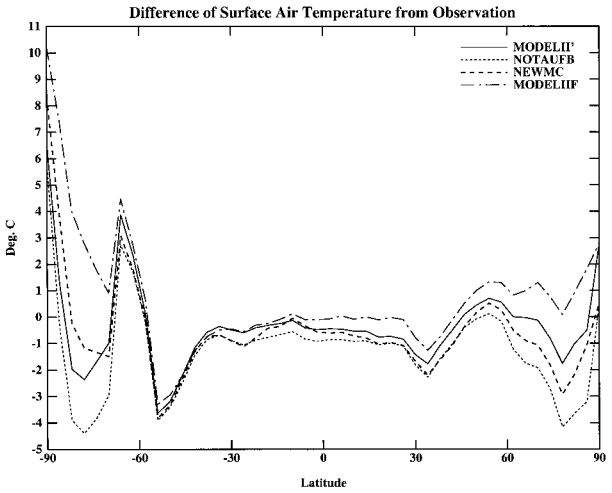

FIG. 1. Zonal mean and annual mean surface air temperature (°C) differences in the current climate between each of the simulations and the climatology of Legates and Willmott (1990).

CRF.) The distributions of the net CRF are similar for MODELII′ and NOANVIL, because the addition of optically thick anvil clouds increases the magnitude of both shortwave (SW) and longwave (LW) CRF by comparable amounts at the top of the atmosphere, consistent with their observed behavior. Net CRF is also similar for the pair NEWMC and MODELIIF because of compensating effects due to less optically thick convective cloud (which reduces the shortwave albedo but also allows for increased longwave emission to space) and the lower altitude of cirrus outside the equatorial region when the new convection scheme (with its weaker and shallower mass fluxes) is used. The net CRF of NOTAUFB is significantly larger (in magnitude) than MODELII′ and NOANVIL, which is a SW-only effect and consistent with more and optically thicker low clouds in NOTAUFB. The net CRF of NEWMC and MODELIIF is very small, and less realistic, in the low latitudes due to the presence of fewer low clouds generated by the Model II large-scale cloud parameterization and the fact that Model II permits only optically thin nonconvective high clouds.

The generation of model clouds is highly dependent on the RH, although cloud cover is not just a function of RH in either Model II or MODELII′. Figure 3a shows the pressure–latitude cross section of RH of the control run for MODELII′; Fig. 4 shows RH differences between the other experiments and MODELII′ in the control climate. The RH of NOTAUFB is similar to MODELII′ (differences are $<3\%$ everywhere). The RH of NOANVIL is less than MODELII′ in the tropical middle and upper troposphere because detrained convective condensate is not available for evaporation. The RHs of NEWMC and MODELIIF are similar; both are drier in the lower troposphere and wetter in the upper troposphere in the low latitudes than MODELII′, more so in

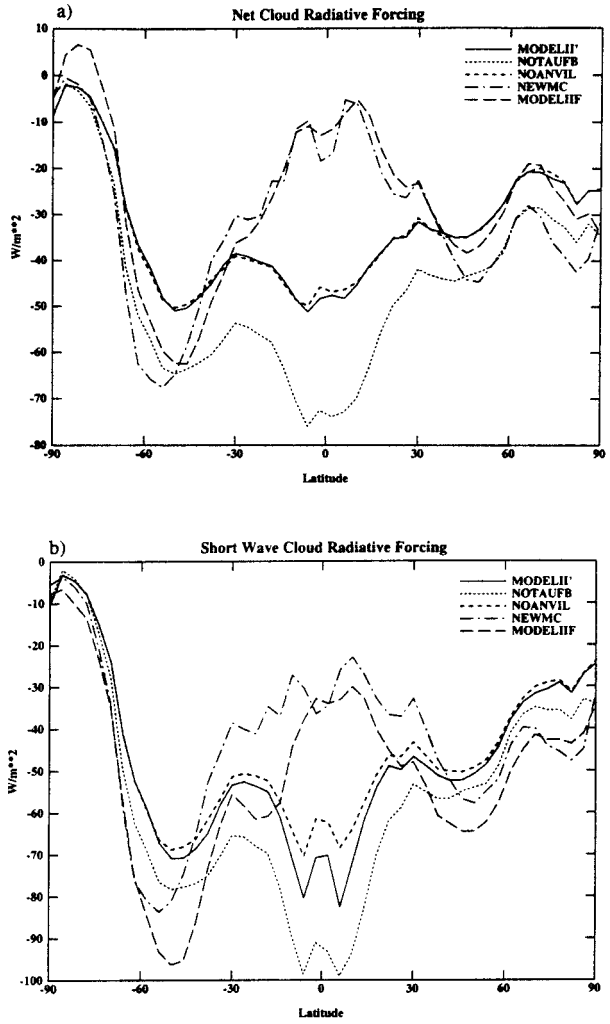

FIG. 2. As in Fig. 1, but for cloud radiative forcing (CRF in W m^{-2}): (a) Net CRF, (b) shortwave CRF, and (c) longwave CRF.

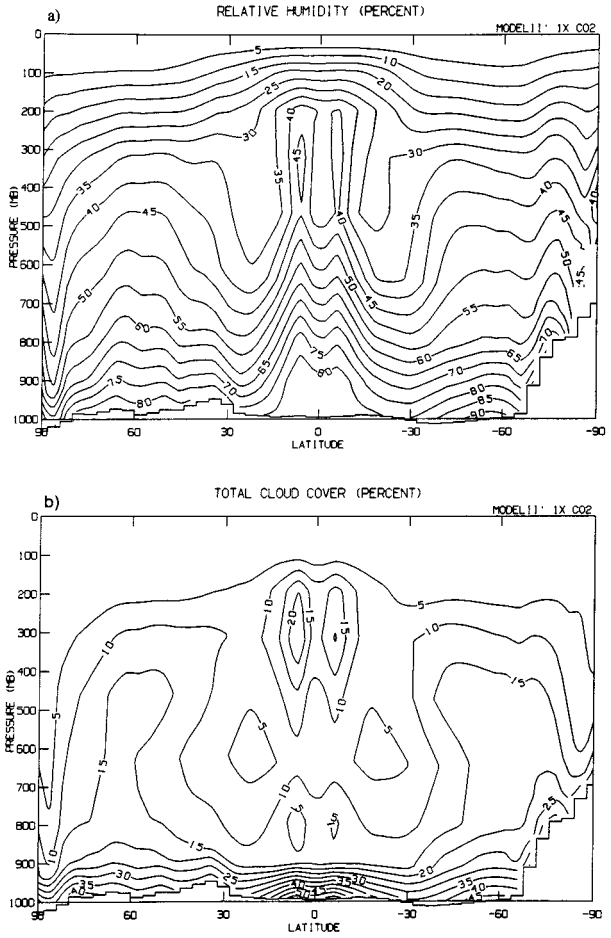

FIG. 3. Pressure–latitude cross sections of (a) RH and (b) cloud cover (%) for MODELII′.

MODELIIF since the Model II moist convection does not have downdrafts that moisten the lower atmosphere. The 5-h time step used in the Model II large-scale cloud parameterization also allows for more moisture to build up in the upper troposphere. The more vigorous convection of MODELIIF also produces higher subtropical upper troposphere RH than the other runs. In middle and high latitudes, on the other hand, NEWMC and MODELIIF are wetter than the other runs.

Figure 3b and 5 show the total cloud cover of the controls. Again, the cloud cover of NOTAUFB is similar to MODELII′ (differences $<3\%$ everywhere). The cloud cover of NOANVIL is smaller than MODELII′ in the tropical upper troposphere due to the omission of anvil clouds. The total cloud cover of NEWMC and MODELIIF are similar; both have much more cirrus cloudiness, but much less tropical low cloudiness, than the runs with prognostic cloud water. In part this can be explained by the differences in the relative humidity profiles of the two models. However, comparison of Figs. 4c,d and 5c,d indicates an additional effect. The different temperature thresholds for condensation rela-

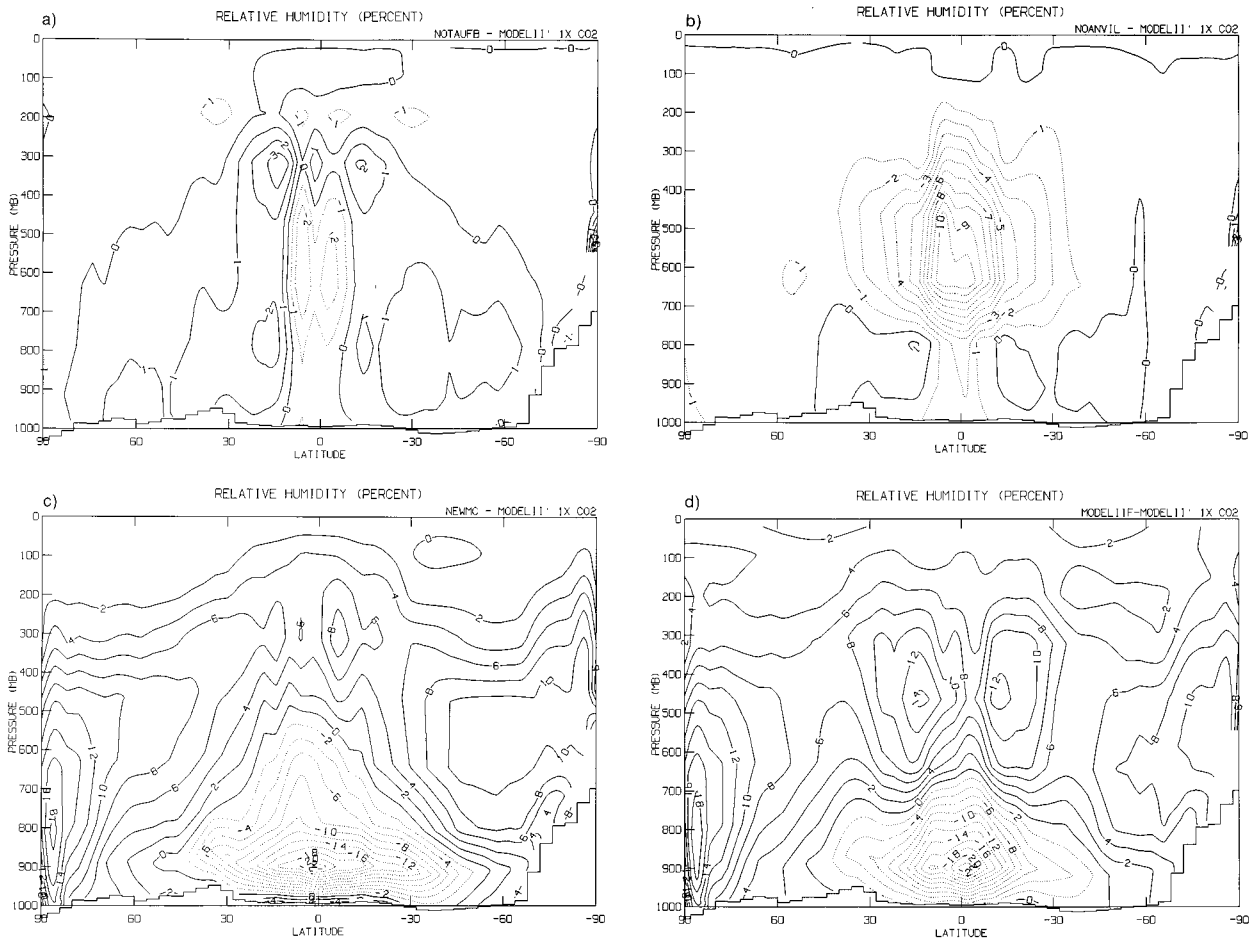

FIG. 4. As in Fig. 3a, but for RH differences between MODELII′ and (a) NOTAUFB, (b) NOANVIL, (c) NEWMC, and (d) MODELIIF. Note that the contour interval for (a) and (b) (1%) differs from that in (c) and (d) (2%).

tive to ice saturation in the diagnostic and prognostic schemes makes it more difficult for cirrus to form below the 300-mb level in the diagnostic scheme, which uses a somewhat artificial −40°C cutoff. Thus, cloud cover is less there, especially in the Tropics, but greater at 200 mb, which receives enhanced vertical transport of vapor that was not condensed at lower levels.

The cloud optical thickness feedback is one of the major concerns of our study, and since the cloud water is closely related to the cloud optical thickness, we further show the cloud water content for MODELII′ and NOANVIL in Fig. 6. The cloud water of NOANVIL is much less than MODELII′ in the tropical upper troposphere in the low latitudes due to the omission of detrainment of convective cloud water to the large-scale clouds. The cloud water of NOTAUFB is similar to MODELII′, and is not shown (however, optical thickness is higher in NOTAUFB, in which cloud water is decoupled from optical properties).

Figure 7 shows the optical thickness (per kilometer of cloud layer depth) of large-scale clouds, calculated as the cloud cover weighted mean $\Sigma (b\tau)/\Sigma b$ since GCM grid boxes are much larger than individual clouds. Optical thicknesses peak in the lower troposphere, particularly in the subtropics and midlatitudes, and decrease monotonically to moderately optically thin values ($\tau \leq 2$) in the upper troposphere. In NOANVIL, there is little latitudinal variation of optical thickness above 700 mb outside the polar regions, while the detrainment of cumulus condensate in MODELII′ causes upper-troposphere clouds to be thicker in the Tropics than at other latitudes. Comparing to the distribution of cloud water content (Fig. 6), we see that anvil detrainment effects are more obvious in the cloud water field than in the optical thickness. This occurs because of the inverse dependence of optical thickness on particle effective radius: ice crystals are parameterized to have larger particle sizes than liquid droplets, and particle size increases with ice water content, and both of these factors mute the effect of large anvil ice content on anvil optical thickness.

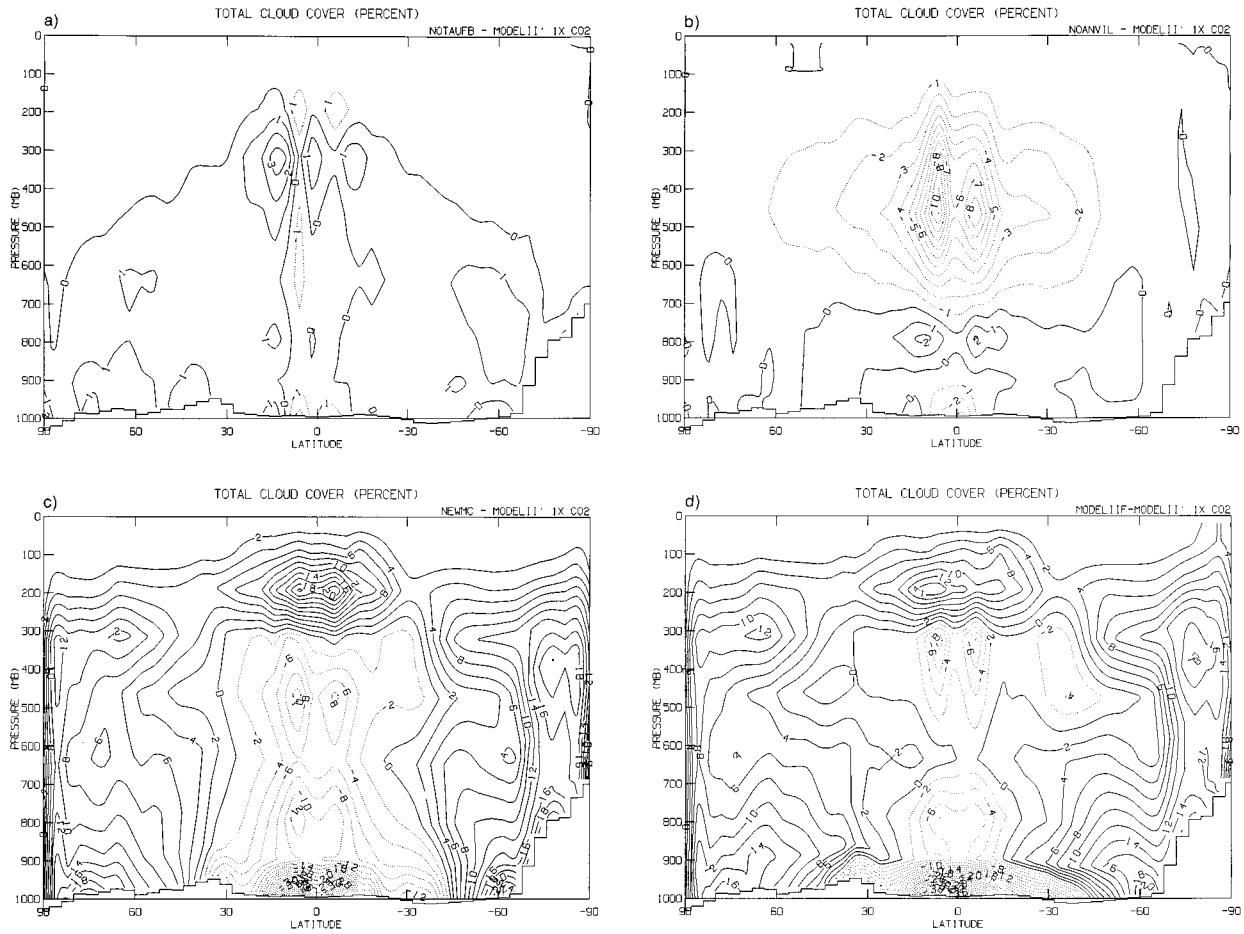

FIG. 5. As in Fig. 3b, but for total cloud cover differences between MODELII′ and (a) NOTAUFB, (b) NOANVIL, (c) NEWMC, and (d) MODELIIF. Note that the contour interval for (a) and (b) (1%) differs from that in (c) and (d) (2%).

4. Climate changes due to doubling CO_2

The climate changes resulting from doubling CO_2 will be primarily discussed in terms of global means and zonal means to limit the discussion. Table 3 shows changes of annual mean and global mean climate parameters. The ΔT_s of MODELIIF is 3.55°C, which is less than the 4.2°C obtained by Hansen et al. (1984) with the same physics at 8° lat × 10° long resolution. This is primarily due to the effect of resolution on cloud generation [discussed further at the end of this section; see also Rind (1988), who analyzed the MODELIIF physics on a 4° lat × 5° long grid but using prescribed sea surface temperatures extrapolated from an 8° lat × 10° long climate change simulation].

When the new moist convection and large-scale cloud parameterizations are used (MODELII′), ΔT_s is reduced to 3.09°C. Without the feedback of optical thickness (NOTAUFB), ΔT_s is further reduced to 2.74°C, suggesting that this feedback is positive overall. Without inclusion of anvil clouds, ΔT_s is increased from 3.09° to 3.7°C, suggesting that anvil clouds of large optical thickness reduce the climate sensitivity. Comparing NOANVIL and NEWMC, we see that the net effect of using the new large-scale cloud parameterization without including the detrainment of convective cloud water is a slight increase of ΔT_s from 3.56° to 3.7°C. Comparing NEWMC and MODELIIF, we see that the net effect on ΔT_s of the new moist convection parameterization without anvil clouds is insignificant. However, we will show later that this is a result of compensating differences in the radiative effects of changes in other climate parameters. The different ΔT_s values are, of course, only partly the result of different cloud feedbacks; interactions with temperature, moisture, sea ice, and snow contribute as well. In section 5 we perform a sensitivity analysis that isolates cloud and clear-sky contributions to the feedback; the clear-sky sensitivity is very similar in all the experiments.

In every run without exception, global low cloud amount and middle cloud amount decrease when CO_2 is doubled, contributing to a positive feedback. With the exception of MODELIIF, high cloud cover increases with climate warming, also contributing to a positive feedback. Table 3 shows that mean cloud-top pressure

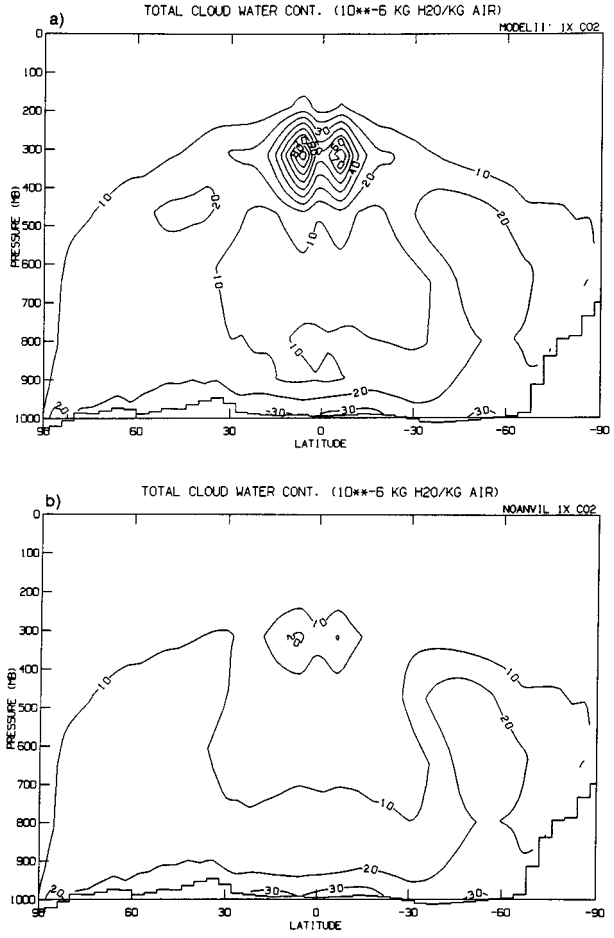

FIG. 6. Pressure–latitude cross sections of cloud water content (10^{-6} kg kg^{-1}): (a) MODELII′, and (b) NOANVIL.

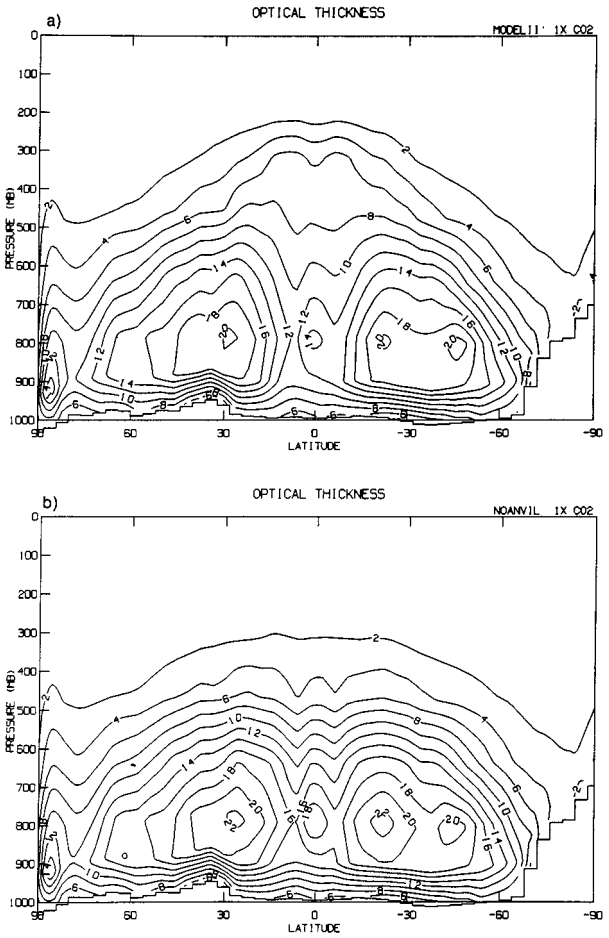

FIG. 7. As in Fig. 6, but for large-scale cloud optical thickness per kilometer: (a) MODELII′, and (b) NOANVIL.

TABLE 3. Changes of global mean and annual mean climate parameters. Here, Q is the absorbed solar radiation, and F is the net longwave radiation. Cloud cover and albedo are in %; radiative and turbulent fluxes are in W m^{-2}.

	MODELII′	NOTAUFB	NOANVIL	NEWMC	MODELIIF
T_s (°C)	3.09	2.74	3.70	3.56	3.55
T_g (°C)	2.98	2.63	3.56	3.45	3.48
Total cloud	−0.76	−0.28	−0.94	0.68	−3.03
Low cloud	−1.42	−0.71	−1.66	−1.08	−2.19
Middle cloud	−0.65	−0.47	−0.20	−0.78	−1.18
High cloud	0.38	0.73	0.76	1.80	−1.58
Cloud height (mb)	−3.2	−5.1	−8.5	−17.2	−3.0
Planetary albedo	−0.35	−0.34	−0.66	−0.54	−0.93
Ground albedo	−0.33	−0.29	−0.37	−0.33	−0.40
Q at TOA	1.19	1.18	2.24	1.83	3.19
F at TOA	−1.44	−1.30	−2.38	−1.78	−2.93
Net radiation at TOA	−0.24	−0.12	−0.13	0.05	0.27
Q at surface	−0.33	−0.25	0.46	−0.02	1.69
F at surface	3.40	3.03	4.16	4.55	3.88
Net radiation at surface	3.07	2.78	4.61	4.53	5.57
Net heat at surface	−0.04	0.02	0.08	−0.06	0.23
Latent heat flux	−4.98	−4.83	−6.70	−7.07	−7.43
Sensible heat flux	1.65	1.83	1.90	2.35	1.88
Precipitation (mm day^{-1})	0.17	0.17	0.23	0.24	0.26
Ocean ice (%)	−1.43	−1.22	−1.62	−1.45	−1.60
Lapse rate (°C km^{-1})	−0.14	−0.08	−0.21	−0.14	−0.22
Precipitable water (mm)	5.84	4.83	7.23	6.48	7.58

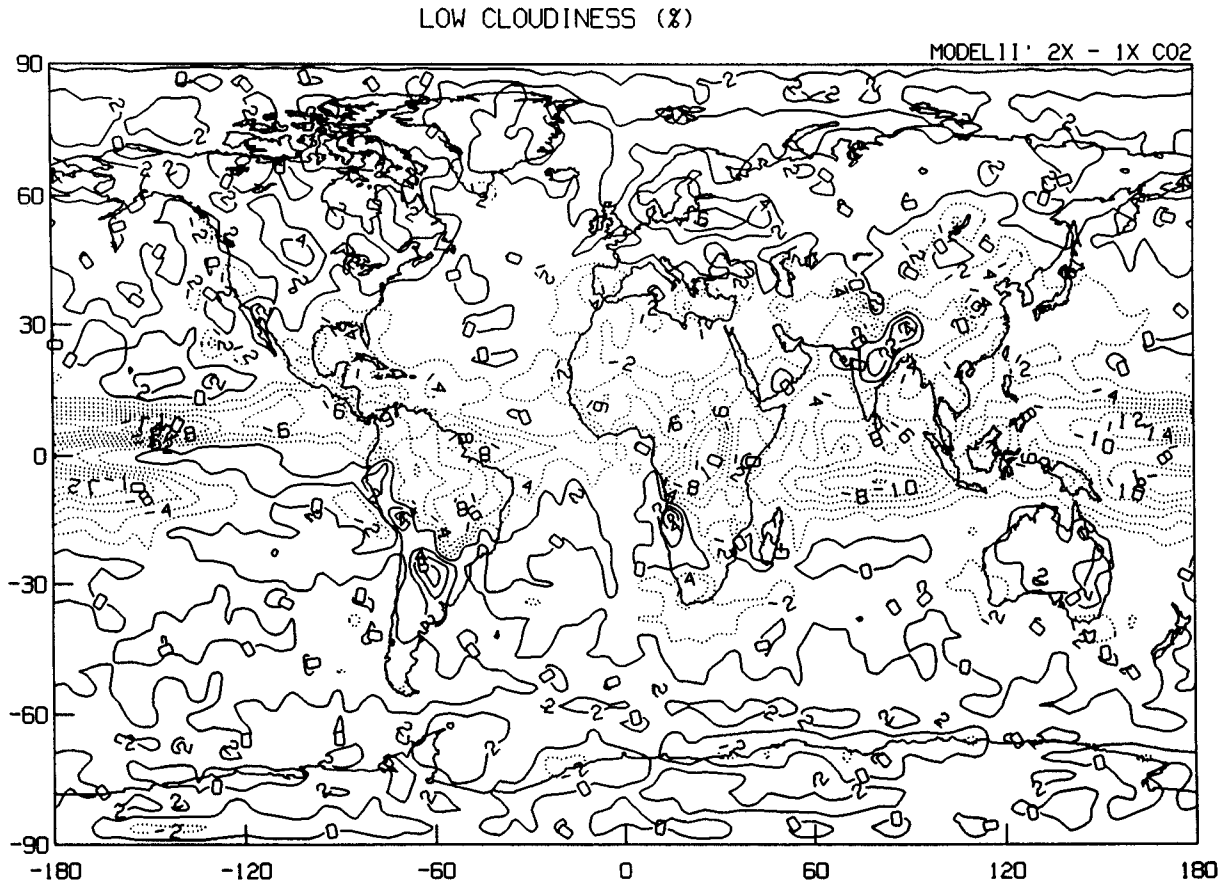

FIG. 8. Geographical distribution of 2 × CO_2 low cloud cover changes (%) for MODELII′.

decreases in all experiments, that is, cloud-height feedback is positive, a common result in GCMs. The combined decrease in low/middle cloud cover and increase in high cloud cover in the warmer climate reflects the enhanced upward transport of moisture by convection and the large-scale circulation, which causes relative humidity to decrease (increase) slightly in the lower (upper) troposphere at most latitudes (cf. Del Genio et al. 1991). The decrease of high clouds in MODELIIF is opposite the behavior of Model II of Hansen et al. (1984); the decrease is restricted to the low latitudes despite the fact that RH increases in the warmer climate [see discussion below and that in Rind (1988)].

The global mean cloud changes in Table 3 appear to be inconsistent with observations that suggest that cloudiness has actually increased in many locations (including the United States, Canada, Europe, Australia, and the former Soviet Union) during the twentieth century (cf. Plantico et al. 1990; Henderson-Sellers 1992). This in turn has led to the suggestion that anthropogenic aerosol effects on low-level clouds may be responsible and may also explain the observed decrease in daily temperature range over the past few decades (cf. Karl et al. 1993; Hansen et al. 1995). Dai et al. (1997), on the other hand, show that the observed cloud cover trends are mostly due to precipitating clouds that usually have low bases but not low tops. Figure 8 shows the geographical distribution of low cloud cover change for MODELII′; the results are fairly similar for all the other runs except MODELIIF, whose overly vigorous convection depletes low cloudiness even more. Although low cloud cover decreases globally, there are significant land–ocean and latitudinal asymmetries: cloud cover feedback is positive over most of the oceans and tropical land, but low cloudiness increases with warming over most middle and high latitude land areas. This is consistent with an enhanced poleward moisture flux by large-scale eddies (not shown) in the warmer climate. It is also consistent with the overall intensification of well-known hydrological cycle features with warming: The hydrologic imbalance between land ($P > E$) and ocean ($E > P$) is strengthened with warming, and the pattern of low cloud changes mimics that of $P - E$ in parts of the world where synoptic baroclinic systems control the hydrologic cycle. These results imply that (a) observed cloudiness trends, which are only available for middle and high latitude land locations, are a biased sample and may not be indicative of global cloud cover feedback; (b) the trends that have been observed may not be due solely to an aerosol indirect effect and may

TABLE 4. Climate sensitivity and TOA radiation budget changes (W m^{-2}) for each of the experiments.

	MODEL-II′	NO-TAUFB	NO-ANVIL	NEW-MC	MODEL-IIF
ΔT_s (°C)	3.09	2.74	3.70	3.56	3.55
ΔQ	1.25	1.17	2.23	2.12	3.10
ΔF	1.49	1.31	2.44	1.93	3.11
ΔQ_c	0.65	0.62	0.85	0.82	0.80
ΔF_c	1.75	0.69	3.10	2.00	1.81
$\Delta(\text{CRF})_{sw}$	0.60	0.55	1.38	1.30	2.29
$\Delta(\text{CRF})_{lw}$	0.25	−0.62	0.67	0.07	−1.30
ΔCRF	0.85	−0.07	2.05	1.37	0.99
λ (°C m^2 W^{-1})	0.74	0.65	0.88	0.85	0.85
λ_c (°C m^2 W^{-1})	0.61	0.66	0.59	0.64	0.68
λ/λ_c	1.20	0.98	1.49	1.33	1.24

partly be a signature of an intensifying global hydrologic cycle.

We note that sea-ice cover decreases with warmer climate roughly in proportion to the magnitude of ΔT_s, contributing to a positive feedback, and that water vapor concentration similarly increases, also a positive feedback, while the lapse rate decreases, contributing to a negative feedback. All these are similar to the results of other doubled CO_2 experiments (cf. Hansen et al. 1984) and will not be discussed further. Reduction of albedo occurs because of the changes in sea-ice and cloud amount. We also note that the net radiation at the top of the atmosphere (TOA) and net surface heating are not strictly zero due to losses in computation and imperfect treatments of physics (cf. Hansen et al. 1984), but the imbalances amount to no more than a 0.1°–0.2°C uncertainty in ΔT_s given the climate sensitivities of the various models (Table 4).

Figure 9 shows the meridional distribution of ΔT_s. Note that the different parameterizations of large-scale clouds and moist convection have a larger impact on ΔT_s in the low/high latitudes than in the midlatitudes. The ΔT_s of NEWMC and MODELIIF are similar to each other, while ΔT_s of MODELII′ is smaller, consistent with their global mean values. The ΔT_s of NOTAUFB is significantly smaller in the low latitudes while ΔT_s of NOANVIL is significantly larger everywhere than that of MODELII′. We also note that ΔT_s increases generally toward the poles. This is a general feature of other climate models (cf. Hansen et al. 1984; Wetherald and Manabe 1986), and is due to the snow/ice-albedo feedback and increases of lapse rate in the convectively stable higher latitudes (cf. Hansen et al. 1984). The larger polar amplification of ΔT_s in the Northern Hemisphere of MODELII′ and NOANVIL is associated with larger increases in the lapse rate (cf. Fig. 10).

Figure 10 shows the pressure–latitude cross sections of changes in temperature for MODELII′, NOANVIL, NEWMC, and MODELIIF. The cross section of NOTAUFB is similar to MODELII′ but with smaller magnitude, and is not shown. Generally, ΔT peaks around 200–300 mb in the Tropics and is negative in the stratosphere, as in previous doubled CO_2 simulations. The peaks of NOANVIL and MODELIIF are larger than those of other experiments, both as a result of larger increases in convective heating. Upper troposphere ΔT is largest at the equator and decreases slightly toward the subtropics. Thus, the Hadley cell can export additional heat from the equatorial region into the subtropics in the warmer climate without strengthening and without requiring T_s to warm more at the equator than in the subtropics. This, in turn, limits static stability increases beneath the subtropical trade inversion. Consequently, increases in subtropical cold pool marine stratus in the warmer climate are modest (Fig. 8), even though planetary boundary layer (PBL) cloud cover increases with stability in our parameterization. In some places where RH decreases with warming, PBL cloudiness decreases instead. [See Miller (1997) for a discussion of the implications of enforcing zero horizontal temperature gradient in a simpler Hadley cell model.]

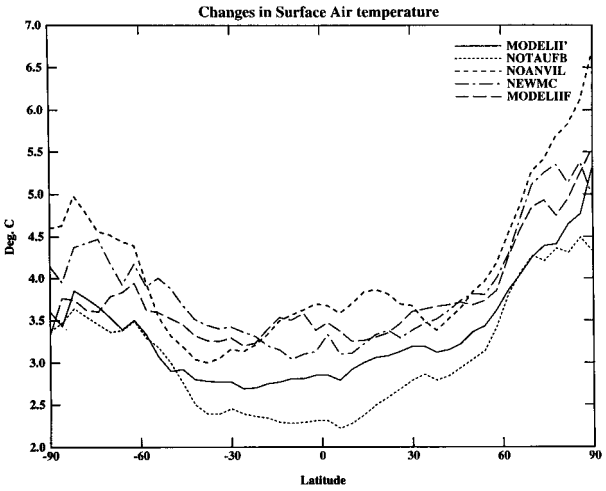

FIG. 9. Zonal mean and annual mean changes in surface air temperature (°C).

The geographic distribution of ΔT_s for MODELII′ (Fig. 11) shows that larger ΔT_s occurs both in the higher latitudes and over continental regions. The latter feature is due to the limited moisture availability over land, which implies that perturbations in the surface radiation budget must be accommodated to a larger extent by increases in the sensible heat flux than by the latent heat flux, which dominates over ocean. Note also that the longitudinal SST gradient across the tropical Pacific weakens slightly in the warmer climate, mostly due to a larger increase in evaporation in the warm pool. The accompanying decrease in Walker cell strength (10%–15%, as indicated by changes in vertical velocity in the upwelling and downwelling branches) limits the magnitude of increases in cumulus anvil reflectivity and thus prevents the occurrence of a strong ''thermostat'' feedback, as pointed out by Del Genio et al. (1996).

To understand the reasons for the different magnitudes and patterns of surface temperature change in the

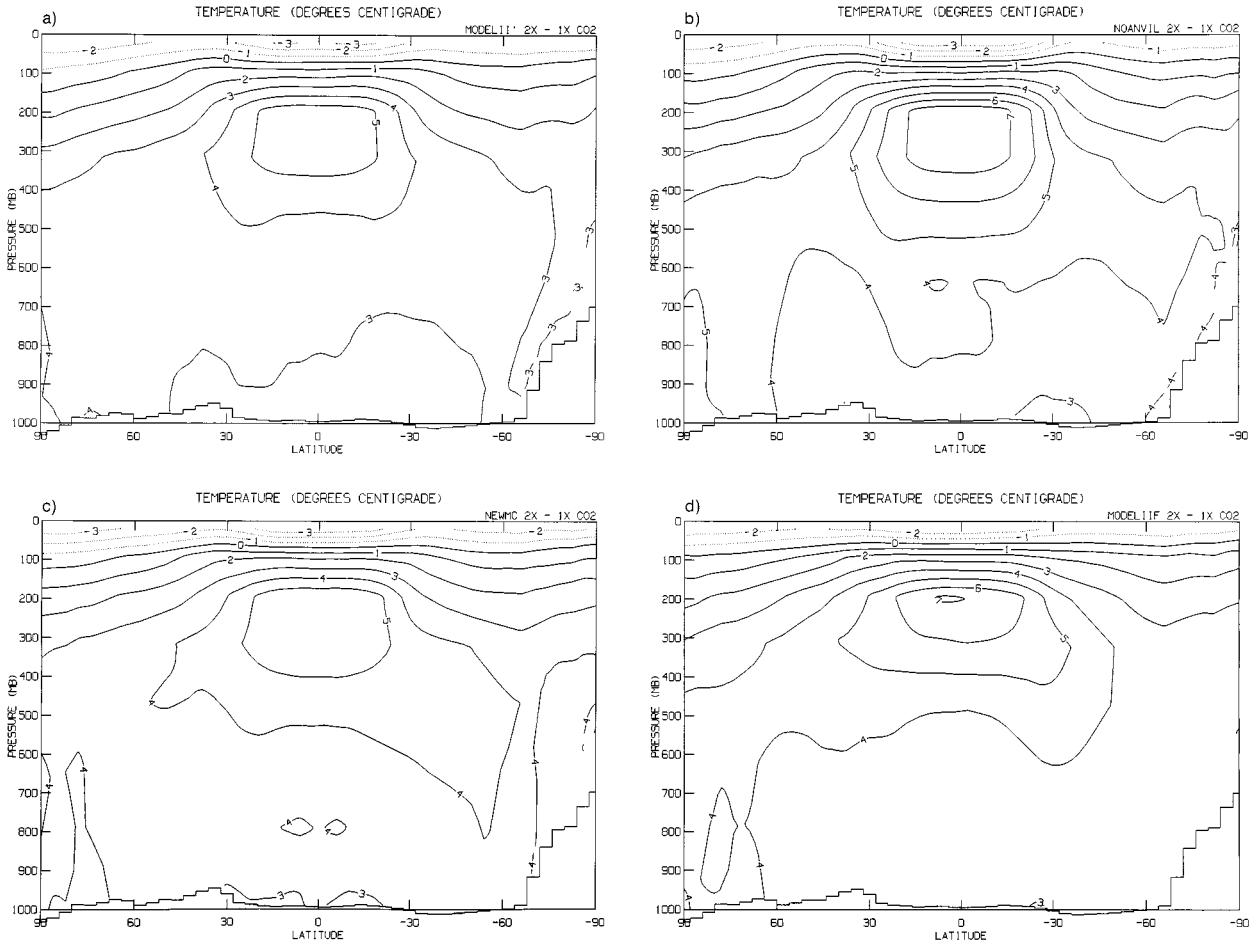

FIG. 10. Pressure–latitude cross sections of changes in temperature (°C): (a) MODELII′, (b) NOANVIL, (c) NEWMC, and (d) MODELIIF.

different experiments, we examine changes in relative humidity, cloud cover, cloud water content, cloud optical thickness, and cloud radiative forcing (Figs. 12–16). The discussion can be organized into three categories: effects of replacing the diagnostic cloud scheme with the prognostic cloud water parameterization (MODELII′ vs NEWMC), effects of optical thickness feedbacks at different altitudes (MODELII′ vs NOTAUFB vs NOANVIL), and effects of changing the moist convection scheme alone (NEWMC vs MODELIIF). In addition, effects of the diagnostic versus prognostic cloud schemes other than those associated with anvils can be isolated by comparing NEWMC and NOANVIL.

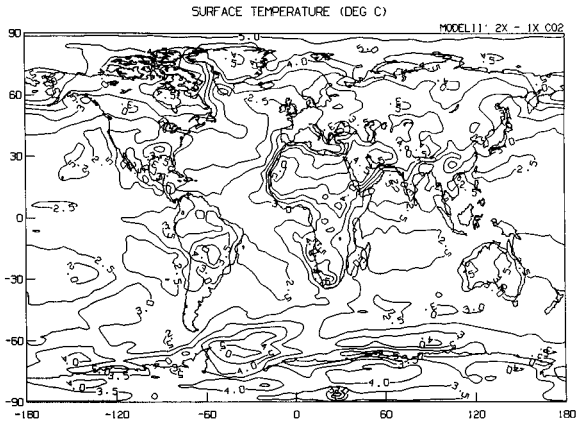

FIG. 11. Geographical distribution of changes in surface air temperature (°C) for MODELII′.

The prognostic cloud scheme reduces climate sensitivity primarily via shortwave effects. Larger decreases in low and middle cloud in midlatitudes in NEWMC (relative to MODELII′, see Figs. 13a,c) allow greater increases in absorbed sunlight (Fig. 16b). Tropical low cloud cover decreases more in MODELII′, but the effect is diminished by concomitant increases in tropical anvil cloud water and optical thickness (Figs. 14a, 15a). Without anvils (NOANVIL), the prognostic scheme actually increases the climate sensitivity instead.

Optical thickness feedbacks for individual cloud types have fairly straightforward effects on climate sensitivity in the GCM. The presence of anvil condensate detrain-

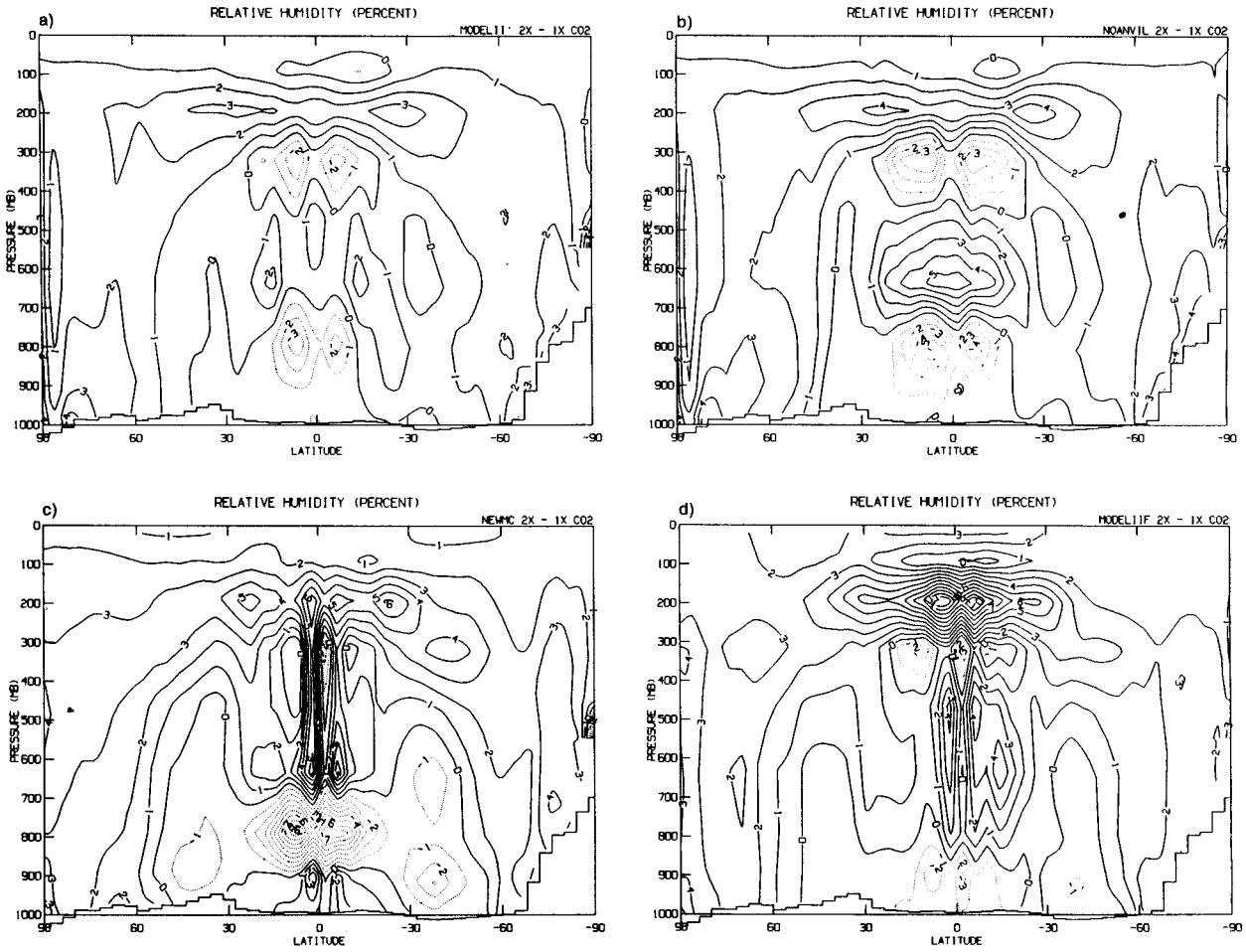

FIG. 12. As in Fig. 10, but for changes in relative humidity: (a) MODELII′, (b) NOANVIL, (c) NEWMC, and (d) MODELIIF.

ment (MODELII′ vs NOANVIL) affects cloud cover in the Tropics in an indirect fashion. The precipitation of ice from anvils (which increases as the anvil ice water content increases in the warmer climate, see Fig. 14a) hastens the formation of precipitation via the Bergeron–Findeisen process in midtroposphere supercooled liquid clouds, preventing a buildup of midlevel tropical cloud (Figs. 13a,b); this by itself would act to increase sensitivity. With anvils, shallow convection in the Tropics is shallower as well, which also limits midlevel increases in relative humidity (Figs. 12a,b) and cloud cover. However, the increase in ice content and optical thickness of the anvils themselves (Figs. 14, 15) as climate warms produce a smaller tropical increase in absorbed shortwave, and this latter effect itself is limited mostly to the Tropics. The increased warming at higher latitudes is the result of a greater increase in poleward moist static energy transport in NOANVIL (9%) relative to MODELII′ (5%).

The suppression of all cloud optical thickness feedbacks (NOTAUFB vs MODELII′) produces the lowest global climate sensitivity of all experiments. The patterns of change of relative humidity, cloud cover, and cloud water in this experiment are all similar to those in MODELII′, but the magnitude of each change is smaller (not shown). The one qualitative exception is that tropical low-level RH and low cloudiness decrease to a lesser extent in NOTAUFB (see discussion below), and thus the positive feedback of decreased low cloud in MODELII′ is diminished. The other important effect on sensitivity is the absence of the optical thickness feedback itself. In MODELII′, optical thickness generally increases for high and middle clouds, but decreases for low clouds, as the climate warms, except at high latitudes (see Fig. 15). The net result for cloud forcing (Fig. 16a) is thus not what one might expect from optical thickness feedbacks, which are often discussed solely in terms of their albedo effects. Instead, the increases/decreases of optical thickness for high/low clouds (Fig. 15) have offsetting effects on shortwave cloud forcing (Fig. 16b), while the increase in high cloud optical thickness increases the emissivity of the thinner clouds and hence their longwave forcing (Fig. 16c). It is then the longwave effect that accounts for

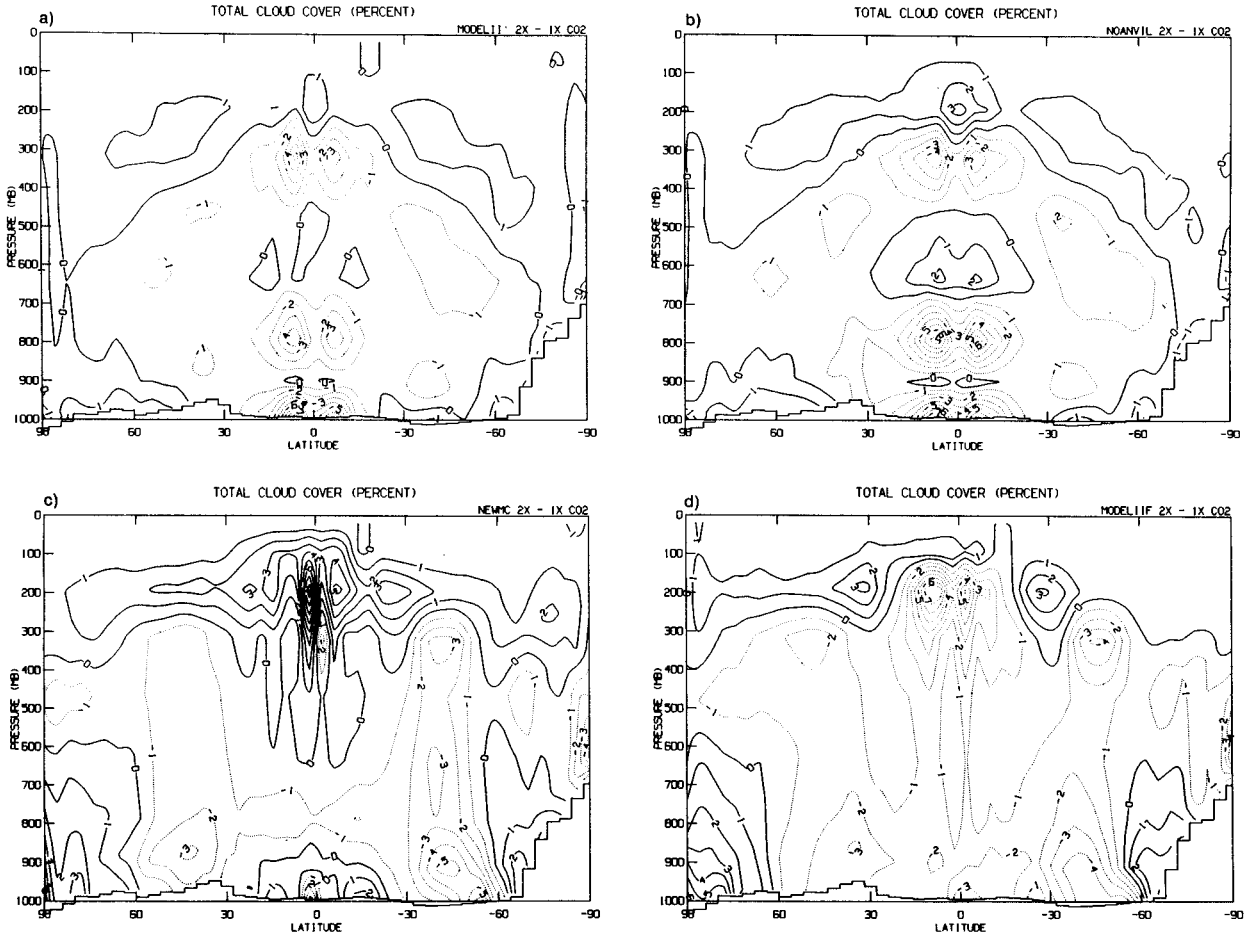

FIG. 13. As in Fig. 10, but for changes in total cloud cover (%): (a) MODELII′, (b) NOANVIL, (c) NEWMC, and (d) MODELIIF.

much of the higher sensitivity of MODELII′ relative to NOTAUFB, and this is felt mostly in the Tropics. The shortwave effect may appear indirectly via its influence on low cloud cover in the Tropics: Tropical surface absorbed SW increases by only 2/3 as much in NOTAUFB as in MODELII′, leading to less strengthening of surface evaporation and greater weakening of sensible heat flux there. As a result, increases in cumulus heating and drying of the tropical boundary layer are smaller in NOTAUFB, and the reduction in low cloud cover is thus more modest.

The new and old moist convection schemes (NEWMC vs MODELIIF) differ in the following three ways: NEWMC has weaker mass fluxes because of its neutral buoyancy closure, so it moistens the upper troposphere less; it represents downdrafts, which cool and moisten the boundary layer and diminish the effects of subsidence there; it allows for entraining as well as nonentraining updrafts and thus produces a wider variety of cloud top heights. The effects of these differences appear to be enhanced in the warmer climate. MODELIIF produces a larger relative humidity increase in the upper troposphere than NEWMC, while the downdrafts in NEWMC actually cause relative humidity to increase in the tropical boundary layer (see Figs. 12c,d).

In general these differences produce corresponding changes in cloud cover with one major exception: tropical high cloud cover decreases dramatically in the warmer climate in MODELIIF (up to 7%) despite as much as 11% relative humidity increase there (Fig. 13d). This counterintuitive result was previously noted by Rind (1988); it is an artifact of a seemingly innocuous feature of the diagnostic Model II large-scale cloud parameterization. In Model II, saturation is assessed relative to water at temperature $> -40°C$ and relative to ice at colder temperature. Since the saturation vapor pressure is greater over liquid than over ice, it is more difficult to make clouds in this model when the temperature rises above $-40°C$. The 200-mb tropical temperatures tend to be 7°–10°C below $-40°C$ in the current climate, so with the greater upper troposphere warming predicted by the stronger convection in MODELIIF, the $-40°C$ threshold is crossed more often in the warmer climate than is the case for NEWMC. The result is an artificial reduction in high cloudiness with warming. The prognostic cloud parameterization uses a gradual

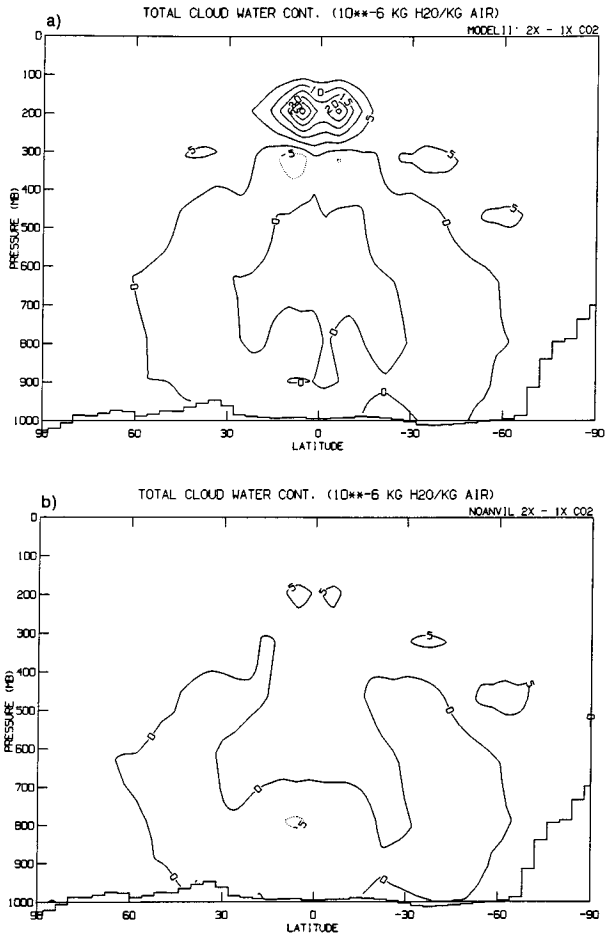

FIG. 14. As in Fig. 10, but for changes in cloud water content (10^{-6} kg kg^{-1}): (a) MODELII′, and (b) NOANVIL.

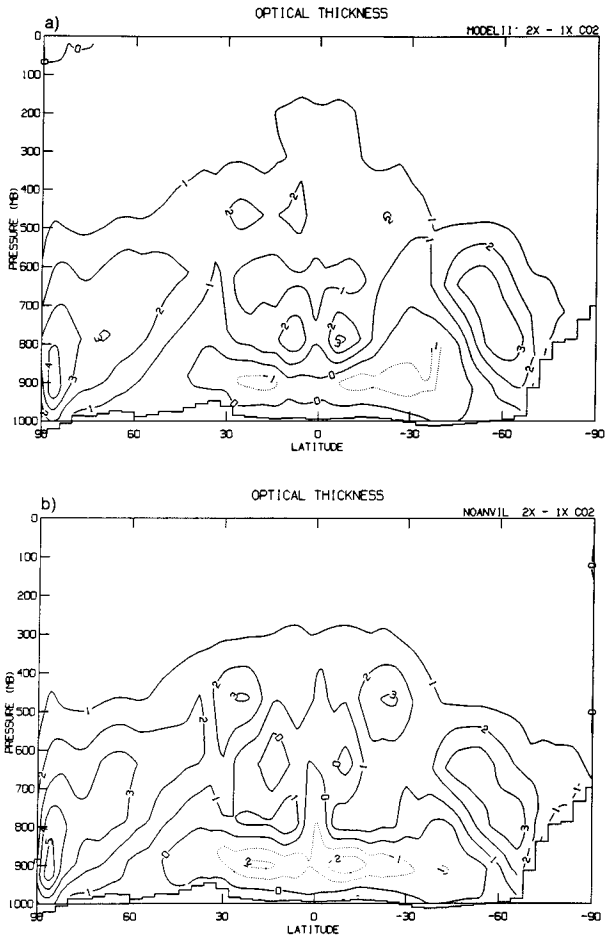

FIG. 15. As in Fig. 10, but for changes in large-scale cloud optical thickness: (a) MODELII′, and (b) NOANVIL.

transition from supercooled liquid to ice over the range 0°C to −40°C and hence is not subject to such behavior.

5. Climate sensitivity and changes in cloud radiative forcing

Cess and Potter (1988) defined a climate sensitivity parameter λ according to

$$\lambda = \Delta T_s/G, \tag{3}$$

where $G = \Delta F - \Delta Q$, the radiative imbalance at the top of the atmosphere. Here, Q and F represent the incoming solar radiation and outgoing longwave radiation at the TOA.

In the case of doubling CO_2, there is an initial radiative perturbation G_o (=4.2 W m^{-2}, see Hansen et al. 1984). Therefore, in general,

$$G = G_o + \Delta F - \Delta Q. \tag{4}$$

At equilibrium, $\Delta F - \Delta Q = 0$ at the TOA, so $G = G_o$.

Cess et al. (1990) used the ratio of λ to λ_C to represent the climate sensitivity of the model resulting from the cloud's feedback, λ_C being the clear-sky sensitivity parameter. One can derive

$$\lambda/\lambda_c = 1 + \Delta\text{CRF}/G, \tag{5}$$

where the CRF is defined as

$$\text{CRF} = (Q - Q_c) - (F - F_c), \tag{6}$$

where Q_c and F_c are clear-sky Q and F, respectively. Method 2 of Ramanathan et al. (1989) is used. For positive cloud feedback, $\lambda/\lambda_c > 1$; for negative cloud feedback, $\lambda/\lambda_c < 1$; when $\lambda/\lambda_c = 0$, cloud feedback is neutral. Note that changes in CRF can be due to changes in both clear and overcast skies; λ/λ_c thus measures both direct cloud effects and correlated effects of temperature and humidity variations in cloudy grid boxes.

Table 4 shows the changes of CRF, λ, λ_c, and λ/λ_c along with ΔT_s for each of the experiments. It is apparent that ΔCRF and λ/λ_c are consistent with ΔT_s in terms of relative magnitude. The meridional variation of ΔCRF (Fig. 16) shows that for all the experiments, the cloud feedback is positive in low and midlatitudes but negative in the polar regions. The simulated polar amplification

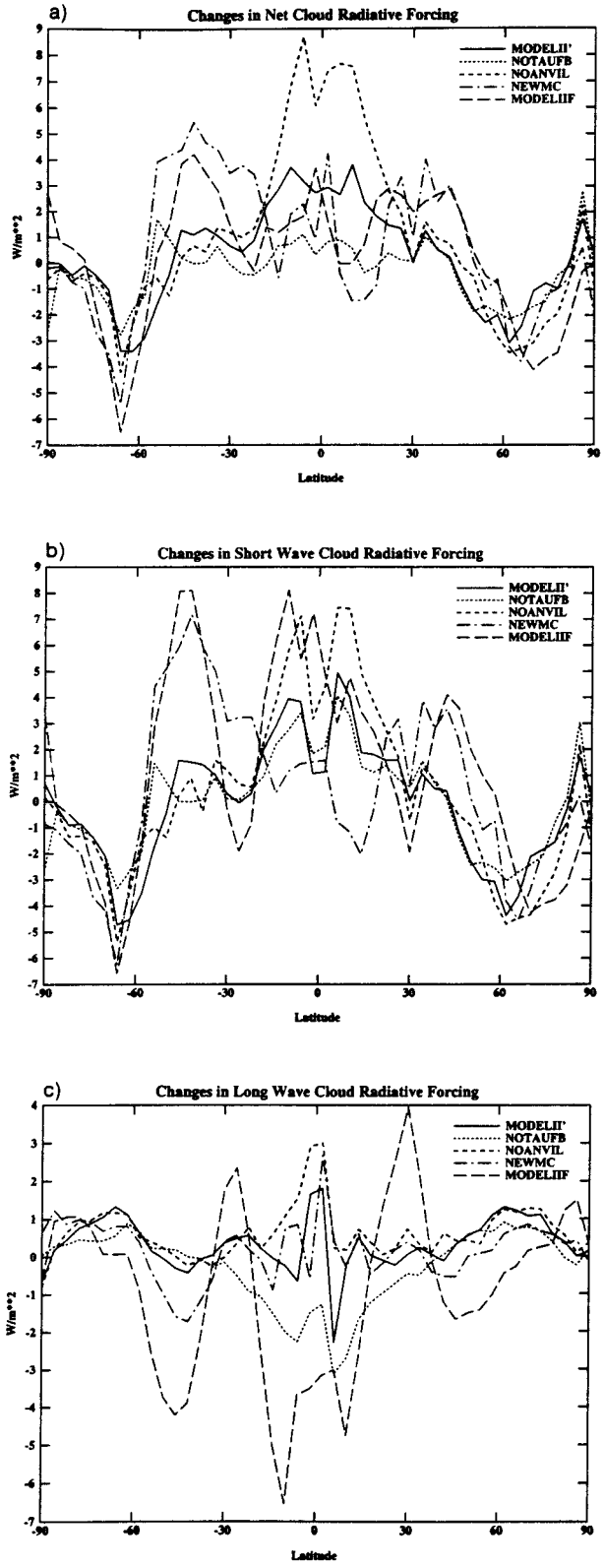

FIG. 16. As in Fig. 9, but for changes in CRF (W m^{-2}): (a) net CRF, (b) shortwave CRF, and (c) longwave CRF.

of ΔT_s is thus the result of positive feedbacks unique to high latitudes (snow/ice–albedo feedback) and increased poleward heat transports (see discussion in section 4), which in the absence of convection contribute to a positive lapse rate feedback at high latitudes (Fig. 10). Except for NOTAUFB, all experiments have a net positive cloud feedback. NOTAUFB is nearly neutral in its cloud feedback. This is consistent with our earlier conclusion that cloud optical thickness feedback is positive in the GCM, as a result of canceling shortwave contributions from high–middle and low clouds and the positive longwave contributions of high clouds. We further note that ΔT_s of NOANVIL (3.7°C) is slightly greater than that of NEWMC (3.56°C); if optical thickness feedback (which is positive in this model) were not included in NOANVIL, we might expect ΔT_s to be slightly smaller than that of NEWMC. This would presumably be evidence of the negative cloud cover feedback due to the phase change of cloud water (Senior and Mitchell 1993). However, as pointed out earlier, our prognostic cloud water parameterization has a much smaller negative effect due to phase change alone; hence, the U.K. Meteorological Office GCM reduction of climate sensitivity from 5.2°C to 2.7°C due to cloud phase effects on lifetime is not duplicated here. Finally, although MODELIIF and NEWMC have almost identical climate sensitivities and cloud feedbacks, they accomplish this via drastically different shortwave and longwave feedback components. It would thus be premature to conclude that climate sensitivity is unaffected by the choice of cumulus parameterization. However, comparison of Figs. 12c and 12d suggests that the new moist convection parameterization would have produced a lower climate sensitivity than MODELIIF if the cloud cover changes in the latter were more consistent with the changes in relative humidity and not influenced so strongly by the −40°C threshold for ice formation. The reason is that NEWMC, whose convection strengthens less than that of MODELIIF in the warmer climate, would under normal circumstances produce less of a positive LW feedback from increased cirrus cloud cover and upper troposphere humidity.

In all versions of the model, SW cloud feedback is positive. Each of the experiments, however, has a smaller SW perturbation than the original Model II physics produces, due to varying combinations of the effects of weaker convection, larger prognostic cloud lifetimes, and cumulus anvil detrainment. Longwave cloud feedbacks vary in sign among the models. Even if we dismiss the MODELIIF result (an artifact caused by the ill-advised on–off switch of liquid versus ice saturation), there is still one more experiment with negative LW feedback (NOTAUFB). This occurs because cloud optical thickness, with the exception of anvils, generally decreases upward. In the absence of optical thickness feedback, an upward shift in mean cloud height implies a decrease in column optical thickness and hence LW emissivity, and in NOTAUFB this effect apparently ex-

ceeds the positive cloud-height feedback itself. Cancellation between feedback effects at different altitudes and latitudes, or between SW and LW feedbacks, result in the different climate sensitivities varying only over a range of 1°C. Here, λ_c is about 0.6, similar to the values obtained by Senior and Mitchell (1993), and varies little among the experiments despite the fact that precipitable water changes differ by up to 50%–60%. The insensitivity of λ_c occurs because experiments with the largest (positive) water vapor feedback are also those with the largest increase in convection and the largest (negative) lapse rate feedback (Table 3). Sea-ice changes contribute to λ_c through ΔQ_c but the differences among the models are not dramatic and scale with the magnitude of ΔT_s.

6. Discussion

We have conducted an ensemble of equilibrium doubled CO_2 experiments with the GISS GCM to explore the effects on climate sensitivity of various aspects of moist convection and stratiform cloud parameterization (cumulus mass flux closure, downdrafts, cloud lifetime, cloud optical thickness feedback, cumulus anvil detrainment). Obviously, the results presented here are model dependent to an extent that is difficult to quantify. Consequently, our results cannot be interpreted as an indicator of either the actual climate sensitivity or its uncertainty. However, the experiments do serve to shed light on a number of common misconceptions about climate GCMs that can be generalized to most models and their predictions of long-term climate change.

1) *Climate models can be validated by comparing their mean state to observations.* If this were true, we would expect that two models with similar mean states would have similar climate sensitivities (and the correct sensitivity if the mean state matched observations). Consider, however, NOANVIL, whose ΔT_s (3.70°C) relative to the baseline MODELII′ (3.09°C) is more different than any of the other experiments that perturb the MODELII′ physics. In the current climate, the net CRF of these two model versions differs by <2 W m^{-2} at all latitudes (Fig. 2a), well within our ability to observe it, and the shortwave and longwave components are each within 10 W m^{-2} at each latitude. In this case, the most touted diagnostic of cloud effects on climate gives us no clue as to how each one will respond to a perturbation. This is true of climate models in general; for example, the GCM intercomparison of Cess et al. (1990) shows no relationship between the CRF simulated by different GCMs and the cloud feedback they predict when perturbed. On the other hand, the larger tropical upper troposphere ice water content of MODELII′ relative to NOANVIL (Fig. 5) does indeed portend the larger climate change in this quantity (Fig. 14), perhaps because it is the result of a single process rather than the net effect of many competing processes. Thus, the only acceptable way to validate a GCM used to predict climate change is to validate the physical processes and relationships responsible for the predicted change. This, in turn, dictates that model–data comparisons should include not only the radiation budget but also cloud and atmosphere physical properties, and that analysis of observations should focus primarily on the nature of current climate variability instead.
2) *Increased ocean evaporation will cause cloud cover to increase in a warming climate.* Many articles about greenhouse warming in the popular press (cf. Stevens 1997) make this assertion. Yet climate GCMs, right or wrong, almost unanimously predict that cloud cover will *decrease* with warming instead (cf. Cess et al. 1990). The claim of increasing cloud cover is usually accompanied by the assumption that cloud cover feedback is negative as a result. In our experiments, however, total cloud cover decreases with warming in all but one case (NEWMC), and in the exception, it is only high cloud (which produces a small positive feedback) that increases. This misconception arises because cloud cover is more closely related to relative humidity than specific humidity and the former depends mostly on convective and large-scale dynamical transports. A physical basis for parameterizing cloud cover does not yet exist, so all such predictions should be viewed with caution, but the view of many nonmodelers on this important aspect of climate change is simply at odds with the actual predictions of the vast majority of existing climate models. In particular, observations of upward trends in cloudiness over the twentieth century, which are restricted to a few midlatitude continental locations, should not necessarily be interpreted as evidence of a global negative cloud feedback; in our GCM at least, such trends coexist with cloud cover decreases over most of the remainder of the world.
3) *The uncertainty in the global climate sensitivity to a doubling of CO_2 is 1.5°–4.5°C, primarily due to uncertainties in cloud feedback.* This statement, found in the most recent Intergovernmental Panel on Climate Change (IPCC 1995) report as well as its 1990 predecessor, almost reflects the full range of climate sensitivity estimates obtained by all GCMs over the past two decades (but with a bias to be discussed below). Implicit in such a statement, then, is an assumption that too little is known about clouds to reject any of the end members of the population. Results such as that of Mitchell et al. (1989), who obtain sensitivities of 1.9°–5.2°C in a single GCM depending on which cloud parameterization they use, support such an assumption. Our results differ dramatically. No matter what we include/exclude from the parameterization, we are unable to change the climate sensitivity by more than 1°C [1.5°C if we include the earlier 8° lat × 10° long result of Hansen

et al. (1984)]. This insensitivity occurs in our model because compensations between cloud feedbacks of different sign involving high versus low clouds, or tropical versus polar clouds, prevent any one aspect of the parameterized physics from making a zero-order difference in the global mean result. The question thus arises as to whether our inability to achieve a low climate sensitivity with this GCM finds any support in observations of cloud variability.

NOANVIL and NOTAUFB illustrate the two most important of the compensating effects that limit our simulated range of sensitivities. Increases in anvil detrainment with warming increase the albedo in the Tropics, but this is offset by the decreasing optical thickness of low clouds. The latter feature of this model is opposite that expected if liquid water content increases adiabatically with temperature. It occurs because at low latitudes liquid water is depleted by precipitation and cloud-top entrainment as temperature rises, while in the subtropics and midlatitudes there is a tendency for low clouds to get physically thinner with warming (Tselioudis et al. 1998). Analyses of International Satellite Cloud Climatology Project (ISCCP) and Special Sensor Microwave Imager (SSM/I) data have shown that the optical thickness (Tselioudis and Rossow 1994) and liquid water path (Greenwald et al. 1995) of low-level clouds do actually decrease with temperature over much of the globe. Tselioudis et al. (1998) find that the GISS GCM qualitatively reproduces the observed temperature dependence of optical thickness in the current climate, and that this temperature dependence is indicative of the cloud optics feedback in climate changes simulated by the model. In addition, Del Genio and Wolf (1998, manuscript submitted to *J. Climate*) find similar behavior in surface remote sensing observations at the Atmospheric Radiation Measurement Program (ARM) southern Great Plains Cloud and Radiation Testbed site.

While these observations do not conclusively prove that cloud optics feedback is positive for low clouds, they cast serious doubt on the assumptions of adiabatic liquid water content and constant geometrical thickness that are responsible for the low end of climate sensitivity estimates. In fact, no GCM has ever predicted a global sensitivity as low as the IPCC 1.5°C lower limit, while several have exceeded the IPCC 4.5°C upper limit. This low bias results from the fact that IPCC assigned greater weight to low sensitivity results from GCMs with early prognostic cloud schemes and discounted high-sensitivity results from models with diagnostic schemes. The observations cited above argue that such a shift is unwarranted and that the lowest sensitivity results resulting from negative low cloud optics feedback are unlikely to be realistic. Furthermore, the lowest sensitivity result of Mitchell et al. (1989) was obtained with unrealistically large ice fall speeds, as these authors point out. With more reasonable ice fallout, and with parameterized Bergeron–Findeisen scavenging of supercooled water, the phase change feedback that contributes to the low sensitivity of that model is likely to be reduced. We therefore suggest that a critical examination of existing climate models supports a higher minimum global climate sensitivity of 2.0°–2.5°C. This is still lower than the lowest sensitivity we attain with the GISS GCM, but is indicative of the lowest sensitivity that would result if a conservative null hypothesis of zero low cloud optics feedback were applied to any existing climate GCM. At the very least, models that cannot reproduce the sense of the ISCCP, SSM/I, and ARM data in this regard should be discounted unless they can demonstrate that observed optical thickness and liquid water path variability in the current climate is irrelevant to the mechanisms that cause cloud optics feedbacks in the models on longer timescales.

It is more difficult to assess the realism of the anvil detrainment feedback in our GCM. Climate changes in upward advection of condensate will depend, at a minimum, on changes in convective available potential energy (CAPE), wind shear, environmental relative humidity, and the drop size distribution in the updraft, and the feedback depends as well on the precipitation and radiative properties of anvils themselves. There are reasons to believe that CAPE will increase with warming (Renno and Ingersoll 1996; Ye et al. 1998), but few guidelines exist for the other parameters; no GCM yet contains a convincing physical parameterization of this process. A semiempirical approach based on statistical relationships derived from satellite data and cloud resolving models may be our best hope of narrowing this major uncertainty. Furthermore, climate changes in tropical anvils are sensitive to changes in the Hadley and Walker circulations and hence the underlying SST gradient. Since the latter can only be predicted in coupled ocean–atmosphere GCMs, the question of climate sensitivity and cloud feedback will have to be addressed in a larger context than that of the parameterization of cloud and convection processes alone (cf. Del Genio et al. 1996).

Acknowledgments. We wish to thank R. Ruedy for providing guidance on using GISS GCM diagnostic programs, especially the programs for computing *Q* flux, and to J. Lerner for the use of GCM plotting programs. This work was supported by the NASA Earth Sciences Modeling and Analysis Program, the NASA FIRE III Project, and the DOE ARM Program.

REFERENCES

Arakawa, A., and W. H. Schubert, 1974: Interaction of a cumulus cloud ensemble with the large-scale environment. Part I. *J. Atmos. Sci.,* **31,** 674–701.

Cess, R. D., and Coauthors, 1990: Intercomparison and interpretation of climate feedback processes in 19 atmospheric general circulation models. *J. Geophys. Res.,* **95,** 16 601–16 615.

——, and Coauthors, 1996: Cloud feedback in atmospheric general circulation models: An update. *J. Geophys. Res.,* **101,** 12 791–12 794.

Dai, A., A. D. Del Genio, and I. Y. Fung, 1997: Clouds, precipitation and temperature range. *Nature,* **386,** 665–666.

Del Genio, A. D., and M.-S. Yao, 1988: Sensitivity of a global climate model to the specification of convective updraft and downdraft mass fluxes. *J. Atmos. Sci.,* **45,** 2641–2668.

——, and ——, 1993: Efficient cumulus parameterization for long-term climate studies: The GISS scheme. *The Representation of Cumulus Convection in Numerical Models, Meteor. Monogr.,* No. 46, Amer. Meteor. Soc., 181–184.

——, A. Lacis, and R. Ruedy, 1991: Simulation of the effect of a warmer climate on atmospheric humidity. *Nature,* **351,** 382–385.

——, M.-S. Yao, W. Kovari, and K.K.-W. Lo, 1996: A prognostic cloud water parameterization for global climate models. *J. Climate,* **9,** 270–304.

Fowler, L. D., D. A. Randall, and S. A. Rutledge, 1996: Liquid and ice cloud microphysics in the CSU general circulation model. Part I: Model description and simulated microphysical processes. *J. Climate,* **9,** 489–529.

Greenwald, T. J., G. L. Stephens, S. A. Christopher, and T. H. Vonder Haar, 1995: Observations of the global characteristics and regional radiative effects of marine cloud liquid water. *J. Climate,* **8,** 2928–2946.

Hansen, J., and L. D. Travis, 1974: Light scattering in planetary atmospheres. *Space Sci. Rev.,* **16,** 527–610.

——, G. Russell, D. Rind, P. Stone, A. Lacis, S. Lebedeff, R. Ruedy, and L. Travis, 1983: Efficient three-dimensional global models for climate studies: Models I and II. *Mon. Wea. Rev.,* **111,** 609–662.

——, A. Lacis, D. Rind, G. Russell, P. Stone, I. Fung, R. Ruedy, and J. Lerner, 1984: Climate sensitivity: Analysis of feedback mechanisms. *Climate Processes and Climate Sensitivity,* J. E. Hansen and T. Takahashi, Eds., Amer. Geophys. Union, 130–163.

——, M. Sato, and R. Ruedy, 1995: Long-term changes of diurnal temperature cycle: Implications about mechanisms of global climate change. *Atmos. Res.,* **37,** 175–209.

——, and Coauthors, 1997: Forcings and chaos in interannual to decadal climate change. *J. Geophys. Res.,* **102,** 25 679–25 720.

Henderson-Sellers, A., 1992: Continental cloudiness changes this century. *Geophys. J.,* **27** (3), 255–262.

IPCC, 1995: *Climate Change 1995: The Science of Climate Change.* Cambridge University Press, 365 pp.

Karl, T. R., and Coauthors, 1993: Asymmetric trends of daily maximum and minimum temperature. *Bull. Amer. Meteor. Soc.,* **74,** 1007–1023.

Legates, D. R., and C. J. Willmott, 1990: Mean seasonal and spatial variability in global surface air temperature. *Theor. Appl. Climatol.,* **41,** 11–21.

Li, Z.-X., and H. LeTreut, 1992: Cloud-radiation feedbacks in a general circulation model and their dependence on cloud modelling assumptions. *Climate Dyn.,* **7,** 133–139.

Miller, R. L., 1997: Tropical thermostats and low cloud cover. *J. Climate,* **10,** 409–440.

Mitchell, J. F. B., C. A. Senior, and W. J. Ingram, 1989: CO_2 and climate: A missing feedback? *Nature,* **341,** 132–134.

Plantico, M. S., T. R. Karl, G. Kukla, and J. Gavin, 1990: Is recent climate change across the United States related to rising levels of anthropogenic greenhouse gases? *J. Geophys. Res.,* **95,** 16 617–16 637.

Ramanathan, V., B. R. Barkstrom, and E. F. Harrison, 1989: Climate and the earth's radiation budget. *Phys. Today,* **42** (5), 22–32.

Renno, N. P., and A. P. Ingersoll, 1996: Natural convection as a heat engine: A theory for CAPE. *J. Atmos. Sci.,* **53,** 572–585.

Rind, D., 1988: Dependence of warm and cold climate depiction on climate model resolution. *J. Climate,* **1,** 965–997.

Roeckner, E., U. Schlese, J. Biercamp, and P. Loewe, 1987: Cloud optical depth feedbacks and climate modelling. *Nature,* **329,** 138–140.

Senior, C. A., and J. F. B. Mitchell, 1993: Carbon dioxide and climate: The impact of cloud parameterization. *J. Climate,* **6,** 393–418.

Smith, R. N. B., 1990: A scheme for predicting layer clouds and their water content in a general circulation model. *Quart. J. Roy. Meteor. Soc.,* **116,** 435–460.

Stevens, W. K., 1997: Computers model world's climate, but how well? *New York Times,* 4 November, p. F1.

Sundqvist, H., 1978: A parameterization scheme for non-convective condensation including prediction of cloud water content. *Quart. J. Roy. Meteor. Soc.,* **104,** 677–690.

Tselioudis, G., and W. B. Rossow, 1994: Global, multiyear variations of optical thickness with temperature in low and cirrus clouds. *Geophy. Res. Lett.,* **21,** 2211–2214.

——, A. D. Del Genio, W. Kovari, and M.-S. Yao, 1998: Temperature dependence of low cloud optical thickness in the GISS GCM: Contributing mechanisms and climate implications. *J. Climate,* **11,** 3268–3281.

Wetherald, R. T., and S. Manabe, 1986: An investigation of cloud cover change in response to thermal forcing. *Climate Change,* **8,** 5–23.

Yao, M.-S., and A. D. Del Genio, 1989: Effects of cumulus entrainment and multiple cloud types on a January global climate model simulation. *J. Climate,* **2,** 850–863.

Ye, B., A. D. Del Genio, and K. K.-W. Lo, 1998: CAPE variations in the current climate and in a climate change. *J. Climate,* **11,** 1997–2015.